Modulating inter-mitochondrial contacts to increase membrane potential for mitigating blue light damage

Yuxin Wang[1,2,†], Kangqiang Qiu[1,†], Weiwei Zou[3,†], Prativa Amom[4], Tushar H. Ganjawala[4], Eugene Lee[1], Zhiqi Tian[1], Xiuqiong Xu[1], Taosheng Huang[3,5], Nien-Pei Tsai[6], Donglu Shi[2,7], Ping Kang[8], Hua Bai[8,*], Amanda L. Zacharias[5,9,*], Kai Zhang[10,*], and Jiajie Diao[1,*]

1. Department of Cancer Biology, University of Cincinnati College of Medicine, Cincinnati, OH 45267, USA.
2. The Materials Science and Engineering Program, Department of Mechanical and Materials Engineering, University of Cincinnati, Cincinnati, OH 45221, USA.
3. Division of Human Genetics, Cincinnati Children's Hospital Medical Center, Cincinnati, OH 45229, USA.
4. Divisions of Developmental Biology and Neonatology and Pulmonary Biology, Cincinnati Children’s Hospital Medical Center, Cincinnati, OH 45229, USA.
5. Department of Pediatrics, University at Buffalo, 1001 Main Street, Buffalo, NY 14203, USA.
6. Department of Molecular & Integrative Physiology, School of Molecular and Cellular Biology, University of Illinois at Urbana-Champaign, Urbana, IL 61801, USA.
7. Department of Biomedical Engineering College of Engineering and Applied Science, University of Cincinnati, Cincinnati, OH 45221, USA.
8. Department of Genetics, Development, and Cell Biology, Iowa State University, Ames, IA 50011, USA.
9. Department of Pediatrics, University of Cincinnati College of Medicine, Cincinnati, OH 45267,

USA

10. Department of Biochemistry, School of Molecular and Cellular Biology, University of Illinois at Urbana-Champaign, Urbana, IL 61801, USA.

†These authors contributed equally to this work.

*Corresponding author. Email: hbai@iastate.edu (H.B.), amanda.zacharias@cchmc.org (A.L.Z.), kaizkaiz@illinois.edu (K.Z.), jiajie.diao@uc.edu (J.D.).

Abstract

Mitochondrial membrane potential (MMP) is essential for mitochondrial functions, yet current methods for modulating MMP lack precise spatial and temporal control. Here, we present an optogenetic system that enables reversible formation of inter-mitochondrial contacts (mito-contacts) with high spatiotemporal precision. Blue light stimulation induces rapid formation of mito-contacts, which fully dissipate upon cessation of illumination. These light-induced mito-contacts can enhance MMP, leading to increased ATP production under stress conditions. Moreover, in human retinal cells and *C. elegans*, high MMP induced by mito-contacts alleviates the deleterious effects of prolonged blue light exposure, restoring energy metabolism and extending organismal lifespan. This optogenetic approach provides a powerful tool for modulating MMP and offers potential therapeutic applications for diseases linked to mitochondrial dysfunction.

Keywords

membrane contact sites, mitochondria, optogenetics

Introduction

Mitochondria, often referred to as the 'powerhouse of the cell', are essential organelles responsible for ATP production and play a critical role in regulating key cellular processes [1,2], including calcium signaling, nutrient sensing, innate immune responses, and programmed cell death [3–7]. The mitochondrial membrane potential (MMP) provides the electrochemical proton gradient that drives ATP synthesis, serving as an intermediate form of stored energy during oxidative phosphorylation [8,9]. Beyond its energetic role, MMP is also essential for maintaining mitochondrial and cellular homeostasis through non-energetic functions, including ion transport, protein import, and mitophagy [10–17]. The dynamic spatial organization of mitochondria is also important when doing these transportation works, forming interconnected networks that enable mitochondria to exchange metabolites, buffer calcium fluctuations, and dynamically adapt to cellular demands. The integrity of mitochondrial network depends on inter-organelle contact sites, which facilitate communication between individual mitochondria and are essential for key processes such as mitochondrial quality control, and homeostasis [18–23].

However, stimulus and stressors, such as excessive reactive oxygen species, can disrupt mitochondrial dynamics by promoting fragmentation, losing mitochondrial contacts, impairing electron transport, and causing MMP depolarization and heterogeneity [24,25]. Depolarization refers to a reduction in the inner mitochondrial membrane potential, indicating a weakened proton motive force and diminished ATP synthesis capacity. In contrast, heterogeneity describes increased variability in MMP among mitochondria, reflecting spatial bioenergetic imbalance and functional asymmetry within the mitochondrial network. Ischemia–reperfusion events frequently trigger prolonged opening of the mitochondrial permeability transition pores, leading to abrupt loss of MMP and widespread mitochondrial dysfunction [26,27]. Similarly, aging-related accumulation of mitochondrial DNA damage

and a decline in mitophagy efficiency lead to a progressive decrease in MMP and increased heterogeneity, ultimately compromising mitochondrial bioenergetics in aged tissues [25,28]. Persistent MMP depolarization impairs ATP production, disrupts calcium homeostasis, and increases susceptibility to apoptosis due to compromised mitochondrial integrity and signaling [29–32]. Moreover, elevated MMP heterogeneity has been linked to inefficient oxidative phosphorylation and metabolic imbalance, contributing to tissue dysfunction and disease progression [33–35]. The disruption or loss of MMP has been linked to pathological conditions, including neurodegenerative disorders, metabolic syndromes, and cardiovascular diseases, where impaired mitochondrial communication drives cellular dysfunction [36–43].

Since MMP is essential for mitochondrial functions, restoring MMP would be critical to maintain energy supply for cells. Several classes of interventions have been developed to preserve or restore MMP under stress conditions. One widely used approach targets the mitochondrial permeability transition pore (mPTP), whose prolonged opening under pathological conditions—such as ischemia-reperfusion injury—causes a sudden collapse of MMP [27]. Uncoupling inhibitors like cyclosporin A inhibit mPTP opening, thereby preventing catastrophic proton leakage and membrane depolarization. However, their effects are context-dependent and limited to conditions where mPTP activation is a primary driver of MMP loss. A second strategy involves mitochondria-targeted antioxidants, such as MitoQ, which aim to neutralize excessive reactive oxygen species (ROS) within mitochondria [44]. ROS accumulation is a major contributor to electron transport chain (ETC) dysfunction and MMP instability. Nonetheless, their efficacy can be compromised by uneven ROS distribution or irreversible oxidative damage, and systemic delivery often leads to off-target effects. A third approach employs metabolic regulators, including nicotinamide riboside (NR) and coenzyme Q10, which boost cellular NAD□ levels or improve ETC substrate availability [45,46]. These agents enhance mitochondrial respiration and indirectly

stabilize MMP. Yet, they do not act on the membrane potential directly and are limited by variable cellular uptake, short half-lives, and the inability to restore MMP when structural mitochondrial damage is present. Collectively, these pharmacological interventions offer partial and often transient support for mitochondrial function. Most lack spatial specificity, act systemically, and fail to correct underlying structural defects, such as the fragmentation of the mitochondrial network or the loss of inter-mitochondrial contacts that are essential for coordinated bioenergetic responses.

Meanwhile, mitochondria experience a range of cellular stresses. With the widespread integration of blue light—a predominant component of light-emitting diodes (LEDs)—into modern life, human exposure to high-energy light has significantly increased, raising concerns about new forms of cellular damage. Indeed, excessive exposure to blue light can cause mitochondrial damage, contributing to serious ocular disorders [47–50]. At the subcellular level, blue light exposure has been shown to disrupt mitochondrial morphology, compromise functional integrity, and reduce MMP [49,51,52]. Therefore, an efficient way to restore MMP would benefit mitochondrial functions upon blue-light damage.

In this study, we present a protein-based optogenetic system applicable to both in vitro and in vivo settings that enables precise and reversible induction of inter-mitochondrial contacts—hereafter referred to as mito-contacts that enhance mitochondrial function, particularly under light-induced stress. The light-induced mito-contacts help maintain high local MMP to support ATP production, thereby preserving mitochondrial activity during prolonged blue light exposure. As the system is activated exclusively by blue light, it provides an *in situ* strategy to mitigate blue light-induced mitochondrial damage. This approach offers valuable potential for both fundamental studies and therapeutic interventions in ophthalmic and other mitochondrial dysfunction-related diseases.

Results

Optogenetic system induces mito-contacts to increase MMP

Inspired by previous studies indicating that nanoscale proximity of a charged membrane or protein condensate to a membrane amplifies the local membrane potential [55,56], we used an optogenetic system, CRY2PHR-mCherry-Miro1TM (Figure 1a), to bring mitochondrial membranes into close contact by light in living cells. The photolyase homology region of cryptochrome (CRY2PHR) [53] was anchored to the outer mitochondrial membrane via the mitochondria-targeting transmembrane domain of Miro1 (Miro1TM) [54]. Upon blue light stimulation (300 $\mu W/cm^2$), CRY2PHR undergoes homo-oligomerization, which brings their bound mitochondria to proximity to form mito-contacts. During this process, the sites of CRY2PHR oligomerization exhibit higher fluorescent signals at light-induced contact sites. As observed under structured illumination microscopy (SIM) (Figure S1), the red fluorescence initially delineated mitochondrial morphology but subsequently formed puncta upon light-activation in less than 5 min (Figure S2).

To better visualize the change of mitochondria before and after optogenetic stimulation, living HeLa cells expressing CRY2PHR-mCherry-Miro1TM were subsequently stained with either MitoTracker™ Deep Red (MTDR) or MitoTracker™ Green (MTG) before and after 20 minutes of blue light exposure. As illustrated in Figure 1b, blue light irradiation significantly increases the interaction between mitochondria. The proportion of mitochondria having one or more mito-contacts increased by nearly 50% following optogenetic stimulation (Figure 1c). Imaging from transmission electron microscopy (TEM) (Figure 1d) further confirmed an approximately 2.5 fold increase in the contact ratio in cells exposed to light compared to those in darkness (Figure 1e). By comparing relative location of contacts (mCherry

puncta) with respect to the morphology of mitochondria (labeled by MTDR), we found various types of mitochondrial contacts (Figure 1f, 1g), such as head-to-head, side-by-side, and head-to-side.

To further characterize the local membrane potential at the mito-contact area, we stained mitochondria with MMP probe Rhodamine 123 (green) and used its average intensity to benchmark MMP at the mito-contract area (Figure 1h). We designed a program to locate light-induced oligomers by distinguishing red puncta from background, circle the peripheral area of the puncta with a diameter of 20 pixels (0.65 μm), enclosing the mito-contact site (Figure 1h and Figure S3a). To calculate MMP, the fluorescent intensity of the green channel was calculated separately for each mito-contact site and background (all green signal excluded in circles) (Figure S3b, c). All sites within a single image were collectively defined as the mito-contact area, and the mean fluorescence intensity across these sites was used to represent the MMP of the mito-contact area. Figure 1i shows the higher MMP at mito-contact area compared to the background. Meanwhile, the CCK-8 test of HeLa cells after blue light treatment confirmed that exposure within 1 h does not cause detectable phototoxicity (Figure S4).

Additionally, to assess the reversibility of the optogenetic system, immediately following blue light stimulation, cells were incubated in darkness for 24 hours and subsequently re-imaged. We observed that most contacted mitochondria separated after incubation in the dark, indicating the reversible control of mito-contacts (Figure S5). When half of a culture dish was covered with aluminum foil during blue light exposure; only the uncovered half resulted in enhanced mito-contacts, demonstrating spatial control (Figure S6). Meanwhile, cells transfected with CRY2PHR-mCherry-Mito1TM under darkness, or non-transfected cells under light illumination, do not show increased mito-contacts to non-transfected cells (Figures S7, S8). These results confirmed that both blue light and photoactivatable proteins are essential

for enhancing mitochondrial interconnection. Furthermore, optogenetically induced mito-contacts were also observed in Michigan Cancer Foundation-7 (MCF-7) cells and neonatal human dermal fibroblasts (HDFn) (Figure S9). Together, these experiments suggest that CRY2PHR-mCherry-Mito1TM can reversibly induce mito-contacts to increase local MMP, consistent with prior findings that close apposition of charged membranes or proteins can markedly enhance membrane potential [55,56].

Mito-contacts increase local MMP to support ATP production upon blue-light damage

To investigate whether optogenetically induced mito-contacts with increased local MMP affect cellular functions, cells were categorized into four groups based on different treatment conditions, as shown in Figure 2a, control (non-transfected) in the dark, control under light exposure, transfected (with CRY2PHR-mCherry-Miro1TM) in the dark, and transfected under light exposure. We then treated cells with continuous blue light for 3 hours - a condition that began to induce significant cell damage (Figure S4). As shown in Figures 2b and S10, mitochondria exposed to blue light for 3 hours exhibited significant fragmentation in non-transfected cells, characterized by an increased number of rounded mitochondria and reduced mitochondrial interactions, both indicative of mitochondrial damage. In contrast, transfected cells showed increased contact ratio under the same light treatment (Figure 2c).

Long-time blue LED light exposure causes mitochondrial depolarization [52], but mito-contacts can maintain relatively high MMP levels at the mito-contact area (Figures 2d, 2e). Damaged cells, particularly those with impaired mitochondria, produce less energy yet require more energy for repair than under normal conditions [57,58]. Since MMP drives ATP synthesis by providing the electrochemical proton gradient [23,59], we quantified ATP production to assess whether locally high MMP would benefit mitochondrial function. As shown in Figure 2f, non-transfected cells exposed to blue light exhibited a

significant reduction in ATP production, confirming mitochondrial impairment. In contrast, cells expressing the optogenetic system showed enhanced ATP production above the basal level - likely reflecting increased energy demands. These findings suggest that mito-contacts increase MMP to boost ATP production and support the recovery of damaged mitochondria.

As mitochondrial fusion is known to support mitochondrial function [60], we conducted a detailed analysis of mitochondrial morphology using SIM imaging. No significant changes in the size of mitochondria were found following optogenetic mito-contact induction (Figure 2g). Instead, the system linked fragmented mitochondria into an extensive network, thereby increasing the number of contact sites among them (Figure S11).

To understand the transcriptional regulation of optogenetically induced mito-contacts, we performed RNA-sequencing (RNA-seq) on the four experimental groups: control in the dark, control with 3-hour light treatment, transfected in the dark, and transfected with 3-hour light treatment. Figure 2h shows the differential gene expression (DEGs) analysis comparing the 3-hour light treatment with dark conditions. The transfected group has 163 DEGs (133 downregulated and 30 upregulated), whereas the non-transfected control group exhibited 540 DEGs (401 downregulated and 139 upregulated). Among the 540 DEGs regulated by blue light, there were 459 unique to the non-transfected group (335 downregulated and 124 upregulated; Figure 2i). The blue light-specific upregulated DEGs were mainly associated with inflammatory signaling pathways (e.g., TNF-α, MAPK, and NF-κB signaling) and lipid and atherosclerosis signaling. In contrast, the downregulated DEGs are linked to gap junction channels, neural plate development, cell migration, and cellular responses to UV exposure. These results suggest that optogenetically induced mito-contacts protect cells from blue light-induced inflammation and

cellular remodeling. Mitochondrial genes were then screened from the whole cell genes (Figure S12a). Long-time blue light exposure caused significant downregulation of several mitochondrial genes, including PET100, SDHAF4, HOGA1. PET100 is located on the mitochondrial inner membrane, exposed to the intermembrane space, and plays an essential role in mitochondrial complex IV maturation and assembly [61,62]. SDHAF4 and HOGA1 localize to the matrix and contribute to complex II assembly and metabolism [62–64]. Notably, in the transfected group, these genes were not significantly downregulated. Besides, we further performed pre-ranked mitochondrial gene expression and annotated their functions using Gene Ontology (GO) analysis and Kyoto Encyclopedia of Genes and Genomes (KEGG) pathway analysis. Only the Control group showed significant changes in gene sets in both analyses (Figure S12b, c). Based on these results, blue light exposure likely disrupts the mitochondrial respiratory chain—the process responsible for ATP production—while mito-contacts help mitigate this effect. This finding explains the reduced ATP levels observed in light-damaged cells and the increased ATP levels in cells with mito-contacts (Figure 2f). KEGG pathway analysis also identified several disease-related terms in the control group but none in the transfected group, suggesting that the mito-contact system may minimize abnormal cellular changes and reduce the risk of light-induced damage or associated diseases. These results inspire a proposed model that mito-contacts facilitate the reintegration of individual mitochondria into the mitochondrial network (Figure 2j), thereby restoring local MMP and enhancing ATP production following light-induced damage.

Mito-contacts preserve MMP for mitochondrial functions upon long-time blue-light eye damage

Considering that the eyes and skin are commonly exposed to natural or artificial blue light throughout the day, the exposure duration for the damage model was extended from hours to a full day [65,66]. We applied the optogenetic mito-contact system to severely damaged human retinal cells (ARPE-19) caused

by prolonged low-intensity blue light exposure [67]. After 24 hours of blue light exposure, the viability of ARPE-19 cells drops below 50%, underscoring the substantial cytotoxicity induced by prolonged blue light exposure (Figure S13). As shown in Figure 3a, long time exposure induced morphological changes in mitochondria within human retinal cells, transforming them from elongated shapes into fragmented, granular forms—hallmarks of mitochondrial damage. In contrast, cells expressing the optogenetic system exhibited networked mitochondrial structures (Figure 3b), further confirming that the system effectively induces mito-contacts under various conditions and consistently increases the contact ratio to approximately 90%.

MMP analysis shows that the mito-contact area consistently exhibited significantly higher fluorescence compared with the background (Figure 3c). Specifically, the fluorescence intensity at mito-contacts was 36.5% higher than the background average (Figure 3d). Functional analysis using the Seahorse assay confirmed that blue light exposure impairs mitochondrial function, whereas light-induced mito-contacts help preserve it (Figures 3e-g). ATP quantification (Figure 3h) further revealed that mitochondria within networks produce higher ATP levels than isolated mitochondria under damaged conditions. These findings suggest that the optogenetic mito-contact system can safeguard mitochondrial function following severe light-induced damage in vitro.

Mito-contact system extends lifespan of *C. elegans* under constant blue-light exposure

To explore the influence of mitochondrial condensation *in vivo*, we applied our optogenetic mito-contact system to *C. elegans* (Figure 4a). When subjected to prolonged blue light exposure, the mitochondria within *C. elegans* exhibited significant fragmentation (Figure 4b), a hallmark of mitochondrial dysfunction [68,69]. However, the optogenetic system successfully reconnected these fragmented

mitochondria (Figure 4c), demonstrating that the optogenetic mito-contact system is functional and effective *in vivo*.

Lifespan is intricately tied to the maintenance of mitochondrial quality control [70]. Building on this finding, we subsequently investigated the effects of mito-contacts on the lifespan of *C. elegans* when they were long-term exposed under blue light. The constant blue light treatment was initiated on Day 1 of adulthood and continued until death. Compared with the untreated control group, animals exposed to blue light exhibited significantly reduced lifespans (Figure 4d). Importantly, no significant differences were observed between the untreated control and untreated transgenic worms (Figure 4e). However, transgenic worms subjected to blue light treatment showed a significant increase in lifespan compared with the non-transfected control group under the same blue light condition (Figure 4f). These results indicate that mito-contact generated by the optogenetic system plays a protective role by mitigating the detrimental effects of blue light exposure, thereby contributing to lifespan extension in damaged organisms.

Discussion

In this study, we reported an optogenetic mito-contact system to increase local MMP. The light-induced mito-contacts foster synergistic interactions among mitochondria, thereby enhancing mitochondrial functions upon blue-light damage. These findings suggest that a mitochondrial membrane contact network could enhance MMP and function as a compensatory mechanism to enhance mitochondrial resilience under environmental stress.

Unlike previous studies that primarily focused on mitochondrial fusion and fission dynamics, our approach highlights an alternative mode of mitochondrial reorganization—mito-conatct—without altering the structure of individual mitochondria. Since not all cells are at the same stage, excessive fusion or fission may benefit abnormal cells while disrupting normal ones. In contrast, increasing mito-contacts does not interfere with cellular activity in normal cells, while supporting damaged mitochondria in restoring their functions (Figures 2, 3). At the subcellular level, individual mitochondria get damaged rapidly due to losing inter- mitochondrial connection and formation of heterogeneity, leading to functional destabilization and a sharp decline in ATP production. Mito-contacts rebuild the network, which benefits mitochondrial transporting electrical signal and exchanging contents. This mechanism helps maintain a local homeostasis and contributes to mitochondrial function. Additionally, high MMP could prevent mitochondrial contents leaking into the cytoplasm, reduces cellular stress and preserves a stable intracellular environment.

On the technical development side, this optogenetic system works only under blue light irradiation, it provides an *in situ* strategy for mitigating mitochondrial damage induced by blue light exposure. Light induced damage with longer exposure times (> 1.5 h) and lower irradiance (< 1 mW/cm^2) was known as Class I or Noell damage which mainly affects photoreceptors, although damage to the retinal pigment epithelium (RPE) can occur with prolonged exposure (> 8 days) [67]. In our study, we designed low-intensity blue light exposure (300 μW/cm^2) across varying durations—ranging from hours to a day and even beyond a month—to simulate different levels of damage and assess the compatibility of the optogenetic system both *in vitro* and *in vivo*. At the cellular level, long-term blue light exposure is known to induce mitochondrial fragmentation and dysfunction, leading to oxidative stress and impaired energy metabolism [71]. We further confirm that prolonged blue light exposure induces mitochondrial

fragmentation and reduces ATP production in retinal cells, as well as shortens the lifespan of *C. elegans*, highlighting the detrimental effects of light-induced damage. Conventional treatments for radiation-induced oxidative stress, such as antioxidants, primarily alleviate symptoms but do not significantly improve mitochondrial function [72,73]. Here, mitochondria undergoing optogenetic mito-contact maintained MMP, provided higher ATP production (Figures 2f, 3h) and extended the lifespan of *C. elegans* exposed to blue light (Figure 4). These findings suggest that mito-contacts hold therapeutic potential for mitigating the effects of prolonged blue light exposure. Again, since the optogenetic system is activated exclusively by blue light, it provides an *in situ* protective mechanism specifically against light-induced damage, addressing a previously unmet need. Moreover, our findings demonstrate the inter-mitochondrial connection enables cells to harness protective benefits from their dysfunctional mitochondria. It is possible that the optogenetically induced mito-contacts resemble those observed in cardiac muscle cells, where clustered mitochondria exhibit coordinated behaviors and functional coupling [76–78].

In conclusion, this optogenetic membrane contact system provides an innovative strategy to study mitochondrial dynamics, offering the advantages of reversibility and precise spatiotemporal control. Additionally, it could also hold promise as a potential therapeutic strategy for ophthalmological, neurodegenerative, and metabolic diseases, which are often associated with mitochondrial fragmentation and energy deficits. For example, modulating membrane contacts between mitochondria and lysosomes has been shown to restore mitochondrial function in cells deficient in mitochondrial fission [79,81], while dynamically regulating membrane contacts between lipid droplets (LDs) and mitochondria can limit lipid transfer from LDs to mitochondria under starvation conditions, thereby offering therapeutic advantages in cancer treatment [82].

Author Contributions

H.B., A.L.Z., K.Z., and J.D. conceived the project. Y.W. and K.Q. carried out cell imaging experiments and analysis, ATP experiment and RNA-seq. W.Z. did the Seahorse experiment. P.A. performed the lifespans and imaging of animals. T.H.G. injected and screened transgenic animals. E.L. did procedures for contact determination. Z.T. assisted with data collection. X.X. drew the schematic. P.K. analyzed RNA-seq data. Y.W., K.Q. and J.D. wrote the manuscript. T.H., N.-P.T., D.S., H.B., A.L.Z., and K.Z. revised the manuscript. All authors participated in discussions on results and in preparing the manuscript.

Notes

The authors declare no competing financial interest.

ACKNOWLEDGMENTS

This work was supported by the National Institutes of Health (NIH R35GM128837 to J.D.; R01GM132438 and R01MH124827 to K.Z.; R01AG058741 and R01AG075156 to H.B.), the National Science Foundation (NSF CAREER 2046984 to H.B.), and the Hevolution Foundation (HF-GRO-23-1199062-14). Additional support was provided by the Cincinnati Children's Research Foundation in the form of a Trustee Award to A.L.Z. We acknowledge the support of the Cincinnati Children's Confocal Imaging Core SCR_022628. Caenorhabditis elegans strain N2 was obtained from the Caenorhabitis Genetics Center project funded by NIH Office of Research Infrastructure Programs (P40 OD010440).

Reference

1. Alshaabi, H., Heininger, M., and Cunniff, B. (2020). Dynamic regulation of subcellular mitochondrial position for localized metabolite levels. J. Biochem. *167*, 109–117. https://doi.org/10.1093/JB/MVZ058.
2. Bulthuis, E.P., Adjobo-Hermans, M.J.W., Willems, P.H.G.M., and Koopman, W.J.H. (2019). Mitochondrial Morphofunction in Mammalian Cells. Antioxidants Redox Signal. *30*, 2066–2109. https://doi.org/10.1089/ARS.2018.7534.
3. Rambold, A.S., Kostelecky, B., Elia, N., and Lippincott-Schwartz, J. (2011). Tubular network formation protects mitochondria from autophagosomal degradation during nutrient starvation. Proc. Natl. Acad. Sci. U. S. A. *108*, 10190–10195. https://doi.org/10.1073/PNAS.1107402108/.
4. Mills, E.L., Kelly, B., and O'Neill, L.A.J. (2017). Mitochondria are the powerhouses of immunity. Nat. Immunol. *18*, 488–498. https://doi.org/10.1038/ni.3704.
5. Martínez-Reyes, I., and Chandel, N.S. (2020). Mitochondrial TCA cycle metabolites control physiology and disease. Nat. Commun. *11*, 1–11. https://doi.org/10.1038/s41467-019-13668-3.
6. Lim, D., Dematteis, G., Tapella, L., Genazzani, A.A., Calì, T., Brini, M., and Verkhratsky, A. (2021). Ca2+ handling at the mitochondria-ER contact sites in neurodegeneration. Cell Calcium *98*, 102453. https://doi.org/10.1016/J.CECA.2021.102453.
7. Chen, Q., Liu, L.Y., Tian, Z., Fang, Z., Wang, K.N., Shao, X., Zhang, C., Zou, W., Rowan, F., Qiu, K., et al. (2023). Mitochondrial nucleoid condensates drive peripheral fission through high membrane curvature. Cell Rep. *42*, 113472. https://doi.org/10.1016/j.celrep.2023.113472.
8. Zorova, L.D., Popkov, V.A., Plotnikov, E.Y., Silachev, D.N., Pevzner, I.B., Jankauskas, S.S., Babenko, V.A., Zorov, S.D., Balakireva, A. V., Juhaszova, M., et al. (2018). Mitochondrial membrane potential. Anal. Biochem. *552*, 50–59. https://doi.org/10.1016/J.AB.2017.07.009.
9. Zorova, L.D., Popkov, V.A., Plotnikov, E.J., Silachev, D.N., Pevzner, I.B., Jankauskas, S.S., Zorov, S.D., Babenko, V.A., and Zorov, D.B. (2018). Functional Significance of the Mitochondrial Membrane Potential. Biochem. Suppl. Ser. A Membr. Cell Biol. *12*, 20–26. https://doi.org/10.1134/S1990747818010129.
10. Korshunov, S.S., Skulachev, V.P., and Starkov, A.A. (1997). High protonic potential actuates a mechanism of production of reactive oxygen species in mitochondria. FEBS Lett. *416*, 15–18. https://doi.org/10.1016/S0014-5793(97)01159-9.
11. Cunha, F.M., Silva, C.C.C. da, Cerqueira, F.M., and Kowaltowski, A.J. (2011). Mild Mitochondrial Uncoupling as a Therapeutic Strategy. Curr. Drug Targets *12*, 783–789. https://doi.org/10.2174/138945011795528778.
12. Scott, I.D., Akerman, K.E., and Nicholls, D.G. (1980). Calcium-ion transport by intact synaptosomes. Intrasynaptosomal compartmentation and the role of the mitochondrial membrane potential. Biochem. J. *192*, 873–880. https://doi.org/10.1042/BJ1920873.
13. Miller, K.E., and Sheetz, M.P. (2004). Axonal mitochondrial transport and potential are correlated. J. Cell Sci. *117*, 2791–2804. https://doi.org/10.1242/JCS.01130.
14. Sato, T.K., Kawano, S., and Endo, T. (2019). Role of the membrane potential in mitochondrial protein unfolding and import. Sci. Rep. *9*, 1–11. https://doi.org/10.1038/S41598-019-44152-Z.
15. Paschen, S.A., and Neupert, W. (2001). Protein Import Into Mitochondria. IUBMB Life *52*, 101–112. https://doi.org/10.1080/15216540152845894.
16. Youle, R.J., and Narendra, D.P. (2010). Mechanisms of mitophagy. Nat. Rev. Mol. Cell Biol. *12*, 9–14. https://doi.org/10.1038/nrm3028.
17. Novak, I. (2012). Mitophagy: A complex mechanism of mitochondrial removal. Antioxidants Redox Signal. *17*, 794–802. https://doi.org/10.1089/ARS.2011.4407.

18. Nunnari, J., and Suomalainen, A. (2012). Mitochondria: In sickness and in health. Cell *148*, 1145–1159. https://doi.org/10.1016/J.CELL.2012.02.035.
19. Chen, H., and Chan, D.C. (2009). Mitochondrial dynamics–fusion, fission, movement, and mitophagy–in neurodegenerative diseases. Hum. Mol. Genet. *18*, R169–R176. https://doi.org/10.1093/HMG/DDP326.
20. Detmer, S.A., and Chan, D.C. (2007). Functions and dysfunctions of mitochondrial dynamics. Nat. Rev. Mol. Cell Biol. *8*, 870–879. https://doi.org/10.1038/nrm2275.
21. Szabadkai, G., Simoni, A.M., Chami, M., Wieckowski, M.R., Youle, R.J., and Rizzuto, R. (2004). Drp-1-dependent division of the mitochondrial network blocks intraorganellar Ca2+ waves and protects against Ca 2+-mediated apoptosis. Mol. Cell *16*, 59–68. https://doi.org/10.1016/j.molcel.2004.09.026.
22. McBride, H.M., Neuspiel, M., and Wasiak, S. (2006). Mitochondria: More Than Just a Powerhouse. Curr. Biol. *16*, R551–R560. https://doi.org/10.1016/J.CUB.2006.06.054.
23. Duchen, M.R. (2000). Mitochondria and calcium: from cell signalling to cell death. J. Physiol. *529*, 57. https://doi.org/10.1111/J.1469-7793.2000.00057.X.
24. Picard, M., Taivassalo, T., Gouspillou, G., and Hepple, R.T. (2011). Mitochondria: isolation, structure and function. J. Physiol. *589*, 4413–4421. https://doi.org/10.1113/JPHYSIOL.2011.212712.
25. Kuznetsov, A. V., and Margreiter, R. (2009). Heterogeneity of Mitochondria and Mitochondrial Function within Cells as Another Level of Mitochondrial Complexity. Int. J. Mol. Sci. *10*, 1911–1929. https://doi.org/10.3390/IJMS10041911.
26. Hausenloy, D.J., and Yellon, D.M. (2004). New directions for protecting the heart against ischaemia-reperfusion injury: Targeting the Reperfusion Injury Salvage Kinase (RISK)-pathway. Cardiovasc. Res. *61*, 448–460. https://doi.org/10.1016/J.CARDIORES.2003.09.024.
27. Halestrap, A.P., and Richardson, A.P. (2015). The mitochondrial permeability transition: A current perspective on its identity and role in ischaemia/reperfusion injury. J. Mol. Cell. Cardiol. *78*, 129–141. https://doi.org/10.1016/J.YJMCC.2014.08.018.
28. Sun, N., Youle, R.J., and Finkel, T. (2016). The Mitochondrial Basis of Aging. Mol. Cell *61*, 654–666. https://doi.org/10.1016/J.MOLCEL.2016.01.028.
29. Hüttemann, M., Lee, I., Pecinova, A., Pecina, P., Przyklenk, K., and Doan, J.W. (2008). Regulation of oxidative phosphorylation, the mitochondrial membrane potential, and their role in human disease. J. Bioenerg. Biomembr. *40*, 445–456. https://doi.org/10.1007/S10863-008-9169-3.
30. Green, D.R., and Reed, J.C. (1999). Mitochondria and apoptosis. Science (80-.). *281*, 1309–1312. https://doi.org/10.1126/SCIENCE.281.5381.1309.
31. Santo-Domingo, J., and Demaurex, N. (2010). Calcium uptake mechanisms of mitochondria. Biochim. Biophys. Acta - Bioenerg. *1797*, 907–912. https://doi.org/10.1016/J.BBABIO.2010.01.005.
32. Ly, J.D., Grubb, D.R., and Lawen, A. (2003). The mitochondrial membrane potential (δψm) in apoptosis; an update. Apoptosis *8*, 115–128. https://doi.org/10.1023/A:1022945107762.
33. Rossignol, R., Gilkerson, R., Aggeler, R., Yamagata, K., Remington, S.J., and Capaldi, R.A. (2004). Energy Substrate Modulates Mitochondrial Structure and Oxidative Capacity in Cancer Cells. Cancer Res. *64*, 985–993. https://doi.org/10.1158/0008-5472.CAN-03-1101.
34. Rovini, A., Heslop, K., Hunt, E.G., Morris, M.E., Fang, D., Gooz, M., Gerencser, A.A., and Maldonado, E.N. (2021). Quantitative analysis of mitochondrial membrane potential heterogeneity in unsynchronized and synchronized cancer cells. FASEB J. *35*, e21148. https://doi.org/10.1096/FJ.202001693R.

35. Glancy, B., and Balaban, R.S. (2012). Role of mitochondrial Ca 2+ in the regulation of cellular energetics. Biochemistry *51*, 2959–2973. https://doi.org/10.1021/BI2018909.
36. Yapa, N.M.B., Lisnyak, V., Reljic, B., and Ryan, M.T. (2021). Mitochondrial dynamics in health and disease. FEBS Lett. *595*, 1184–1204. https://doi.org/10.1002/1873-3468.14077.
37. Suárez-Rivero, J.M., Villanueva-Paz, M., Cruz-Ojeda, P.D. la, Mata, M.D. la, Cotán, D., Oropesa-Ávila, M., Lavera, I. De, Álvarez-Córdoba, M., Luzón-Hidalgo, R., and Sánchez-Alcázar, J.A. (2016). Mitochondrial Dynamics in Mitochondrial Diseases. Dis. 2017, Vol. 5, Page 1 *5*, 1. https://doi.org/10.3390/DISEASES5010001.
38. Shah, S.I., Paine, J.G., Perez, C., and Ullah, G. (2019). Mitochondrial fragmentation and network architecture in degenerative diseases. PLoS One *14*, e0223014. https://doi.org/10.1371/JOURNAL.PONE.0223014.
39. Pokharel, M.D., Garcia-Flores, A., Marciano, D., Franco, M.C., Fineman, J.R., Aggarwal, S., Wang, T., and Black, S.M. (2024). Mitochondrial network dynamics in pulmonary disease: Bridging the gap between inflammation, oxidative stress, and bioenergetics. Redox Biol. *70*, 103049. https://doi.org/10.1016/J.REDOX.2024.103049.
40. Dorn, G.W. (2015). Mitochondrial dynamism and heart disease: changing shape and shaping change. EMBO Mol. Med. *7*, 865–877. https://doi.org/10.15252/EMMM.201404575.
41. Wang, X., Su, B., Lee, H.G., Li, X., Perry, G., Smith, M.A., and Zhu, X. (2009). Impaired Balance of Mitochondrial Fission and Fusion in Alzheimer's Disease. J. Neurosci. *29*, 9090–9103. https://doi.org/10.1523/JNEUROSCI.1357-09.2009.
42. Chen, Q., Camara, A.K.S., Stowe, D.F., Hoppel, C.L., and Lesnefsky, E.J. (2007). Modulation of electron transport protects cardiac mitochondria and decreases myocardial injury during ischemia and reperfusion. Am. J. Physiol. - Cell Physiol. *292*, 137–147. https://doi.org/10.1152/AJPCELL.00270.2006.
43. Szendroedi, J., Phielix, E., and Roden, M. (2011). The role of mitochondria in insulin resistance and type 2 diabetes mellitus. Nat. Rev. Endocrinol. *8*, 92–103. https://doi.org/10.1038/nrendo.2011.138.
44. Smith, R.A.J., Hartley, R.C., and Murphy, M.P. (2011). Mitochondria-targeted small molecule therapeutics and probes. Antioxidants Redox Signal. *15*, 3021–3038. https://doi.org/10.1089/ARS.2011.3969/ASSET/IMAGES/LARGE/FIGURE8.JPEG.
45. Gomes, A.P., Price, N.L., Ling, A.J.Y., Moslehi, J.J., Montgomery, M.K., Rajman, L., White, J.P., Teodoro, J.S., Wrann, C.D., Hubbard, B.P., et al. (2013). Declining NAD+ induces a pseudohypoxic state disrupting nuclear-mitochondrial communication during aging. Cell *155*, 1624–1638. https://doi.org/10.1016/J.CELL.2013.11.037/ATTACHMENT/3067D54E-F8A4-4B9F-B454-B62F74CFF956/MMC2.PDF.
46. Trammell, S.A.J., and Brenner, C. (2013). Targeted, LCMS-based metabolomics for quantitative measurement of NAD+ metabolites. Comput. Struct. Biotechnol. J. *4*, e201301012. https://doi.org/10.5936/CSBJ.201301012/ASSET/969C618E-A340-4A2A-9E37-AE75C4C05A4D/MAIN.ASSETS/FX1.JPG.
47. Wang, L., Yu, X., Zhang, D., Wen, Y., Zhang, L., Xia, Y., Chen, J., Xie, C., Zhu, H., Tong, J., et al. (2023). Long-term blue light exposure impairs mitochondrial dynamics in the retina in light-induced retinal degeneration in vivo and in vitro. J. Photochem. Photobiol. B Biol. *240*, 112654. https://doi.org/10.1016/J.JPHOTOBIOL.2023.112654.
48. Yan, Y., Wu, Y., Zhao, Y., Yang, Y., An, G., Liu, Z., and Qi, D. (2025). A review on eye diseases induced by blue light: pathology, model, active ingredients and mechanisms. Front. Pharmacol. *16*, 1513406. https://doi.org/10.3389/FPHAR.2025.1513406.

49. Tao, J.X., Zhou, W.C., and Zhu, X.G. (2019). Mitochondria as Potential Targets and Initiators of the Blue Light Hazard to the Retina. Oxid. Med. Cell. Longev. *2019*, 6435364. https://doi.org/10.1155/2019/6435364.
50. Li, J.Y., Zhang, K., Xu, D., Zhou, W.T., Fang, W.Q., Wan, Y.Y., Yan, D.D., Guo, M.Y., Tao, J.X., Zhou, W.C., et al. (2018). Mitochondrial fission is required for blue light-induced apoptosis and mitophagy in retinal neuronal R28 cells. Front. Mol. Neurosci. *11*, 412389. https://doi.org/10.3389/FNMOL.2018.00432/BIBTEX.
51. Godley, B.F., Shamsi, F.A., Liang, F.Q., Jarrett, S.G., Davies, S., and Boulton, M. (2005). Blue light induces mitochondrial DNA damage and free radical production in epithelial cells. J. Biol. Chem. *280*, 21061–21066. https://doi.org/10.1074/JBC.M502194200.
52. Hao, W., Zhao, C., Li, G., Wang, H., Li, T., Yan, P., and Wei, S. (2023). Blue LED light induces cytotoxicity via ROS production and mitochondrial damage in bovine subcutaneous preadipocytes. Environ. Pollut. *322*, 121195. https://doi.org/10.1016/J.ENVPOL.2023.121195.
53. Zhang, K., and Cui, B. (2015). Optogenetic control of intracellular signaling pathways. Trends Biotechnol. *33*, 92–100. https://doi.org/10.1016/j.tibtech.2014.11.007.
54. Duan, L., Che, D., Zhang, K., Ong, Q., Guo, S., and Cui, B. (2015). Optogenetic control of molecular motors and organelle distributions in cells. Chem. Biol. *22*, 671–682. https://doi.org/10.1016/j.chembiol.2015.04.014.
55. Bu, B., Tian, Z., Li, D., and Ji, B. (2016). High transmembrane voltage raisedby close contact initiates fusion pore. Front. Mol. Neurosci. *9*, 231245. https://doi.org/10.3389/FNMOL.2016.00136/BIBTEX.
56. Gurunian, A., Lasker, K., and Deniz, A.A. (2025). Biomolecular Condensates Can Induce Local Membrane Potentials. Small *22*, e09591. https://doi.org/10.1002/SMLL.202509591;WEBSITE:WEBSITE:PERICLES;REQUESTEDJOURNAL:JOURNAL:16136829;WGROUP:STRING:PUBLICATION.
57. Milanese, C., Bombardieri, C.R., Sepe, S., Barnhoorn, S., Payán-Goméz, C., Caruso, D., Audano, M., Pedretti, S., Vermeij, W.P., Brandt, R.M.C., et al. (2019). DNA damage and transcription stress cause ATP-mediated redesign of metabolism and potentiation of anti-oxidant buffering. Nat. Commun. *10*, 1–16. https://doi.org/10.1038/s41467-019-12640-5.
58. Flood, D., Lee, E.S., and Taylor, C.T. (2023). Intracellular energy production and distribution in hypoxia. J. Biol. Chem. *299*. https://doi.org/10.1016/J.JBC.2023.105103.
59. Romero-Garcia, S., and Prado-Garcia, H. (2019). Mitochondrial calcium: Transport and modulation of cellular processes in homeostasis and cancer (Review). Int. J. Oncol. *54*, 1155–1167. https://doi.org/10.3892/IJO.2019.4696.
60. Guo, Y., Zhang, H., Yan, C., Shen, B., Zhang, Y., Guo, X., Sun, S., Yu, F., Yan, J., Liu, R., et al. (2023). Small molecule agonist of mitochondrial fusion repairs mitochondrial dysfunction. Nat. Chem. Biol. *19*, 468–477. https://doi.org/10.1038/s41589-022-01224-y.
61. Church, C., Chapon, C., and Poyton, R.O. (1996). Cloning and characterization of PET100, a gene required for the assembly of yeast cytochrome c oxidase. J. Biol. Chem. *271*, 18499–18507. https://doi.org/10.1074/JBC.271.31.18499/ASSET/9939B616-EB46-4053-8C9A-AC6B2BF69C31/MAIN.ASSETS/GR9.JPG.
62. Vidoni, S., Harbour, M.E., Guerrero-Castillo, S., Signes, A., Ding, S., Fearnley, I.M., Taylor, R.W., Tiranti, V., Arnold, S., Fernandez-Vizarra, E., et al. (2017). MR-1S Interacts with PET100 and PET117 in Module-Based Assembly of Human Cytochrome c Oxidase. Cell Rep. *18*, 1727–1738. https://doi.org/10.1016/J.CELREP.2017.01.044/ATTACHMENT/88A41DA2-D6EC-4D41-B7A2-4E9B20940A56/MMC3.PDF.

63. Li, B., Zhang, C., Cao, L., Chen, P., Liu, T., Gao, H., Wang, L., Yan, B., and Tong, L. (2023). Brain Functional Representation of Highly Occluded Object Recognition. Brain Sci. *13*, 1387. https://doi.org/10.3390/BRAINSCI13101387.
64. Cochat, P., and Rumsby, G. (2013). Primary Hyperoxaluria. N. Engl. J. Med. *369*, 649–658. https://doi.org/10.1056/NEJMRA1301564.
65. Nash, T.R., Chow, E.S., Law, A.D., Fu, S.D., Fuszara, E., Bilska, A., Bebas, P., Kretzschmar, D., and Giebultowicz, J.M. (2019). Daily blue-light exposure shortens lifespan and causes brain neurodegeneration in Drosophila. npj Aging Mech. Dis. *5*, 1–8. https://doi.org/10.1038/s41514-019-0038-6.
66. Cougnard-Gregoire, A., Merle, B.M.J., Aslam, T., Seddon, J.M., Aknin, I., Klaver, C.C.W., Garhöfer, G., Layana, A.G., Minnella, A.M., Silva, R., et al. (2023). Blue Light Exposure: Ocular Hazards and Prevention—A Narrative Review. Ophthalmol. Ther. *12*, 755. https://doi.org/10.1007/S40123-023-00675-3.
67. Chakravarthy, H., Georgyev, V., Wagen, C., Hosseini, A., and Matsubara, J. (2024). Blue light-induced phototoxicity in retinal cells: implications in age-related macular degeneration. Front. Aging Neurosci. *16*, 1509434. https://doi.org/10.3389/FNAGI.2024.1509434.
68. Johnson, J., Mercado-Ayon, E., Mercado-Ayon, Y., Dong, Y.N., Halawani, S., Ngaba, L., and Lynch, D.R. (2021). Mitochondrial dysfunction in the development and progression of neurodegenerative diseases. Arch. Biochem. Biophys. *702*, 108698. https://doi.org/10.1016/J.ABB.2020.108698.
69. Wai, T., García-Prieto, J., Baker, M.J., Merkwirth, C., Benit, P., Rustin, P., Rupérez, F.J., Barbas, C., Ibañez, B., and Langer, T. (2015). Imbalanced OPA1 processing and mitochondrial fragmentation cause heart failure in mice. Science (80-.). *350*. https://doi.org/10.1126/SCIENCE.AAD0116.
70. Sharma, A., Smith, H.J., Yao, P., and Mair, W.B. (2019). Causal roles of mitochondrial dynamics in longevity and healthy aging. EMBO Rep. *20*. https://doi.org/10.15252/EMBR.201948395.
71. Guo, K.-X., Huang, C., Wang, W., Zhang, P., Li, Y., Liu, Z.-Y., Wang, M.-S., Guo, K.-X., Huang, C., Wang, W., et al. (2020). Oxidative stress and mitochondrial dysfunction of retinal ganglion cells injury exposures in long-term blue light. Int. J. Ophthalmol. *13*, 1854–1863. https://doi.org/10.18240/IJO.2020.12.03.
72. Ouyang, X., Yang, J., Hong, Z., Wu, Y., Xie, Y., and Wang, G. (2020). Mechanisms of blue light-induced eye hazard and protective measures: a review. Biomed. Pharmacother. *130*, 110577. https://doi.org/10.1016/J.BIOPHA.2020.110577.
73. Sasaki, M., Yuki, K., Kurihara, T., Miyake, S., Noda, K., Kobayashi, S., Ishida, S., Tsubota, K., and Ozawa, Y. (2012). Biological role of lutein in the light-induced retinal degeneration. J. Nutr. Biochem. *23*, 423–429. https://doi.org/10.1016/J.JNUTBIO.2011.01.006.
74. Sloat, S.R., and Hoppins, S. (2023). A dominant negative mitofusin causes mitochondrial perinuclear clusters because of aberrant tethering. Life Sci. Alliance *6*. https://doi.org/10.26508/LSA.202101305.
75. Chevrollier, A., Bonnard, A.A., Ruaud, L., Gueguen, N., Perrin, L., Desquiret-Dumas, V., Guimiot, F., Becker, P.H., Levy, J., Reynier, P., et al. (2024). Homozygous MFN2 variants causing severe antenatal encephalopathy with clumped mitochondria. Brain *147*, 91–99. https://doi.org/10.1093/BRAIN/AWAD347.
76. Amchenkova, A.A., Bakeeva, L.E., Chentsov, Y.S., Skulachev, V.P., and Zorov, D.B. (1988). Coupling membranes as energy-transmitting cables. I. Filamentous mitochondria in fibroblasts and mitochondrial clusters in cardiomyocytes. J. Cell Biol. *107*, 481–495.

https://doi.org/10.1083/JCB.107.2.481.
77. Kurz, F.T., Aon, M.A., O'Rourke, B., and Armoundas, A.A. (2017). Functional implications of cardiac mitochondria clustering. Adv. Exp. Med. Biol. *982*, 1–24. https://doi.org/10.1007/978-3-319-55330-6_1.
78. Sun, Y., Kim, H.J., and Moon, M.J. (2020). Fine structure of the cardiac muscle cells in the orb-web spider Nephila clavata. Appl. Microsc. *50*, 1–8. https://doi.org/10.1186/S42649-020-00030-X.
79. Qiu, K., Xu, X., Zhang, K., and Diao, J. (2025). Alternating Cellular Functions by Optogenetic Control of Organelles. Methods Mol. Biol. *2840*, 175–183. https://doi.org/10.1007/978-1-0716-4047-0_13.
80. Qiu, K., Zou, W., Fang, Z., Wang, Y., Bell, S., Zhang, X., Tian, Z., Xu, X., Ji, B., Li, D., et al. (2023). 2D MoS2 and BN Nanosheets Damage Mitochondria through Membrane Penetration. ACS Nano *17*, 4716–4728. https://doi.org/10.1021/ACSNANO.2C11003/.
81. Qiu, K., Zou, W., Fang, H., Hao, M., Mehta, K., Tian, Z., Guan, J.L., Zhang, K., Huang, T., and Diao, J. (2022). Light-activated mitochondrial fission through optogenetic control of mitochondria-lysosome contacts. Nat. Commun. *13*, 1–9. https://doi.org/10.1038/s41467-022-31970-5.
82. Bai, Q., Shao, X., Xia, Q., Yang, S., Gao, Y., Sun, K., Li, J., Wang, X., Tian, Z., Chen, X., et al. (2025). Optogenetic engineering of lipid droplet spatial organization for tumor suppression. Trends Biotechnol. *43*, 2838–2855. https://doi.org/10.1016/j.tibtech.2025.06.002.

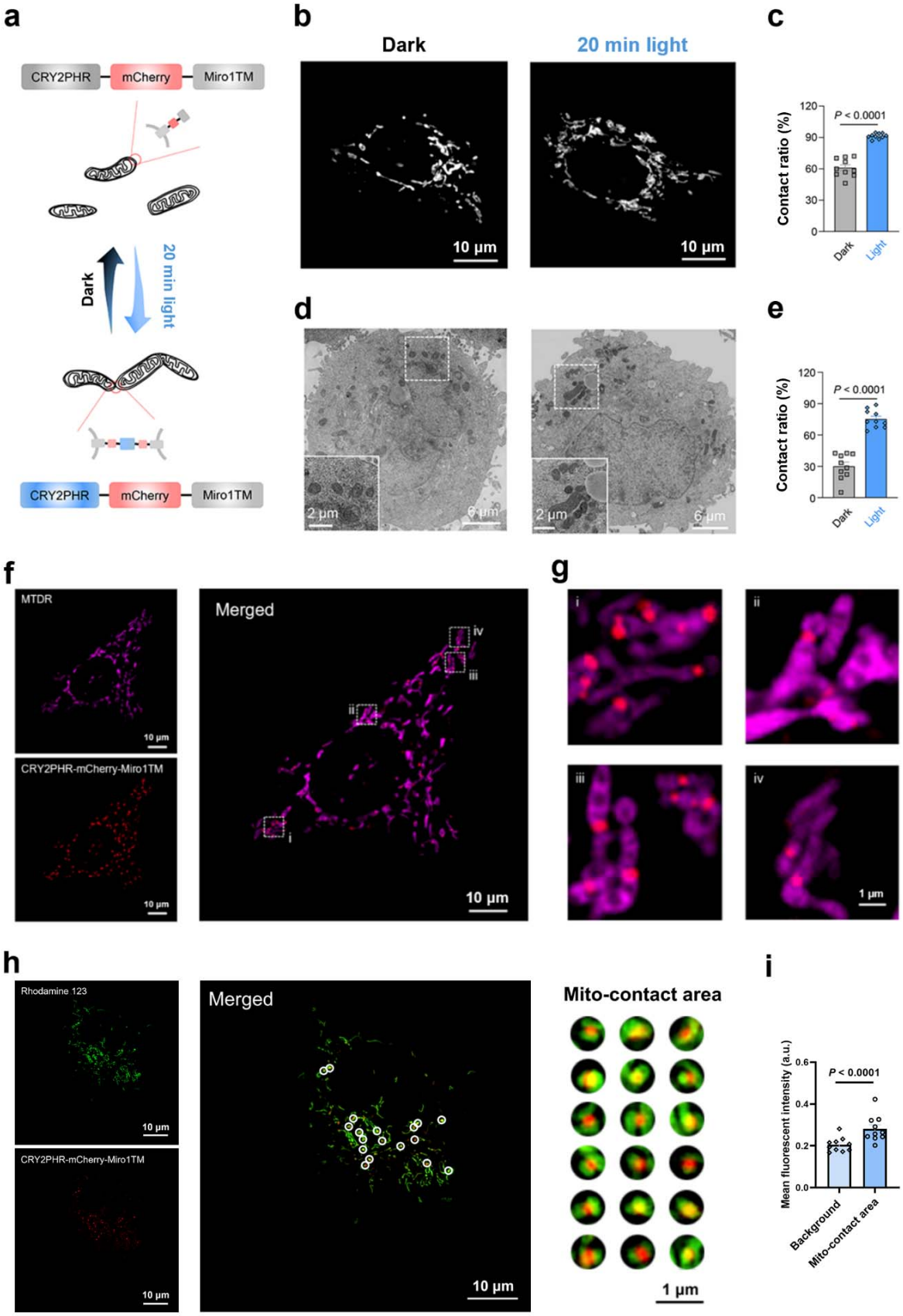
a
CRY2PHR
mCherry
Miro1TM
Dark
20 min light
CRY2PHR
mCherry
Miro1TM
b
Dark
20 min light
10 μm
10 μm
c
Contact ratio (%)
P < 0.0001
Dark
Light
d
2 μm
6 μm
2 μm
6 μm
e
Contact ratio (%)
P < 0.0001
Dark
Light
f
MTDR
10 μm
CRY2PHR-mCherry-Miro1TM
10 μm
Merged
iv
iii
ii
i
10 μm
g
i
ii
iii
iv
1 μm
h
Rhodamine 123
10 μm
CRY2PHR-mCherry-Miro1TM
10 μm
Merged
10 μm
Mito-contact area
1 μm
i
Mean fluorescent intensity (a.u.)
P < 0.0001
Background
Mito-contact area

Figure 1. Optogenetic system induces mito-contacts to increase MMP

(a) Schematic representation of the blue light induced mitochondrial contacts. The light-sensitive proteins CRY2PHR were anchored to mitochondria via the specific organelle-targeting transmembrane domain Miro1TM. Under blue light illumination, the CRY2PHR interacted with each other to form mito-contact. Meanwhile, the fluorescent protein mCherry served as a marker of the plasmid's expression.

(b) Representative SIM images of living HeLa cells expressing CRY2PHR-mCherry-Miro1TM and stained with MitoTracker™ Green (MTG). The left one was incubated in the dark condition and the right one was under blue light exposure with the power density of 300 $\mu W/cm^2$ for 20 min.

(c) The percentage contact ratio of mitochondria from SIM images of HeLa cells corresponding to (b). Data are given as $M \pm SEM$ (n = 10).

(d) Representative TEM images of HeLa cells expressing CRY2PHR-mCherry-Miro1TM. The left one was incubated in the dark condition and the right one was under blue light exposure with the power density of 300 $\mu W/cm^2$ for 20 min. **(e)** The percentage contact ratio of mitochondria from the TEM images of HeLa corresponding to (d). Data are given as $M \pm SEM$ (n = 10).

(f) Representative SIM images of a living HeLa cell expressing CRY2PHR-mCherry-Miro1TM and staining MitoTracker™ Deep Red FM (MTDR) with blue light exposure at 300 $\mu W/cm^2$ for 20 min.

(g) The zoom in images of different mito-contact area from (f). The red dots were light induced CRY2PHR aggregate.

(h) Representative SIM images of transfected + 20 min light exposed HeLa cells staining with Rhodamine 123 to reveal real-time mitochondial membrane potatioal (MMP) in a live cell and the zoom in images are mito-contact area.

(i) Relative MMP between whole cells and mito-contact area (CRY2PHR aggerate dots enriched area) corresponding to (h). Data are given as $M \pm SEM$ (n = 10).

Statistical differences between the experimental groups were analyzed using a double-tailed Student's t test. All P values less than 0.05 were considered to indicate statistical significance.

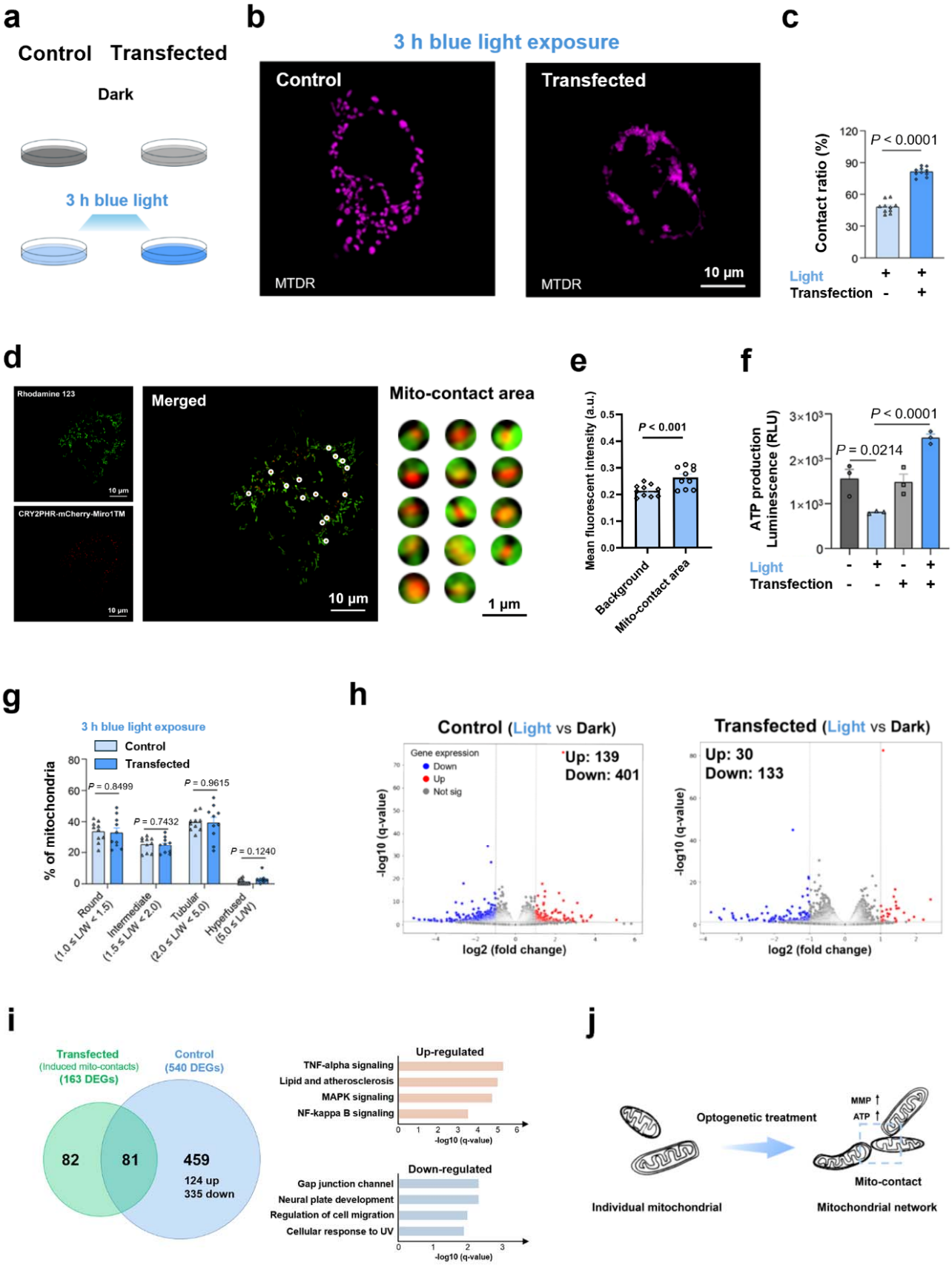
a
Control
Transfected
Dark
3 h blue light
b
3 h blue light exposure
Control
Transfected
MTDR
MTDR
10 μm
c
Contact ratio (%)
P < 0.0001
Light
Transfection
d
Rhodamine 123
CRY2PHR-mCherry-Miro1TM
Merged
10 μm
Mito-contact area
1 μm
e
Mean fluorescent intensity (a.u.)
P < 0.001
Background
Mito-contact area
f
ATP production Luminescence (RLU)
P < 0.0001
P = 0.0214
Light
Transfection
g
3 h blue light exposure
Control
Transfected
% of mitochondria
P = 0.8499
P = 0.7432
P = 0.9615
P = 0.1240
Round (1.0 ≤ L/W < 1.5)
Intermediate (1.5 ≤ L/W < 2.0)
Tubular (2.0 ≤ L/W < 5.0)
Hyperfused (5.0 ≤ L/W)
h
Control (Light vs Dark)
Gene expression
Down
Up
Not sig
Up: 139
Down: 401
-log10 (q-value)
log2 (fold change)
Transfected (Light vs Dark)
Up: 30
Down: 133
-log10 (q-value)
log2 (fold change)
i
Transfected
(Induced mito-contacts)
(163 DEGs)
Control
(540 DEGs)
82
81
459
124 up
335 down
Up-regulated
TNF-alpha signaling
Lipid and atherosclerosis
MAPK signaling
NF-kappa B signaling
-log10 (q-value)
Down-regulated
Gap junction channel
Neural plate development
Regulation of cell migration
Cellular response to UV
-log10 (q-value)
j
Optogenetic treatment
MMP ↑
ATP ↑
Mito-contact
Individual mitochondrial
Mitochondrial network

Figure 2. Mito-contacts increase local MMP to support ATP production upon blue-light damage

(a) Schematic representation of four groups of treatment for HeLa cells.

(b) Representative SIM images of living HeLa cells exposed under blue light of 300 μW/cm^2 for 3 h. The left one was from the control group and the right one was from the transfected group.

(c) The percentage contact ratio of mitochondria from SIM images of HeLa cells corresponding (b). Data are given as $M \pm SEM$ (n = 10).

(d) Representative SIM images of transfected + 3 h light exposed HeLa cells staining with Rhodamine 123 to reveal real-time MMP in a live cell and the zoom in images are mito-contact area.

(e) Relative MMP between whole cells and mito-contact area (CRY2PHR aggerate dots enriched area) corresponding to (d). Data are given as $M \pm SEM$ (n = 10).

(f) The ATP production of HeLa cells with different treatments. Data are given as $M \pm SEM$ (n = 3).

(g) Quantitative analysis of mitochondrial morphology in (b). Data are given as $M \pm SEM$ (n = 10).

(h) The differential gene expression between dark and 3h light treated cells from RNA-sequence data of all four groups HeLa cells. The left one was Control groups (light vs dark), mapping the 139 upregulated genes (red) and 401 downregulated genes (blue); the right one was Transfected groups (light vs dark), mapping the 30 upregulated genes (red) and 133 downregulated genes (blue).

(i) The blue light-specific regulated DEGs and related pathways.

(j) Schematic representation of mito-contact maintaining functions.

Statistical differences between the experimental groups were analyzed using a double-tailed Student's t test. All P values less than 0.05 were considered to indicate statistical significance.

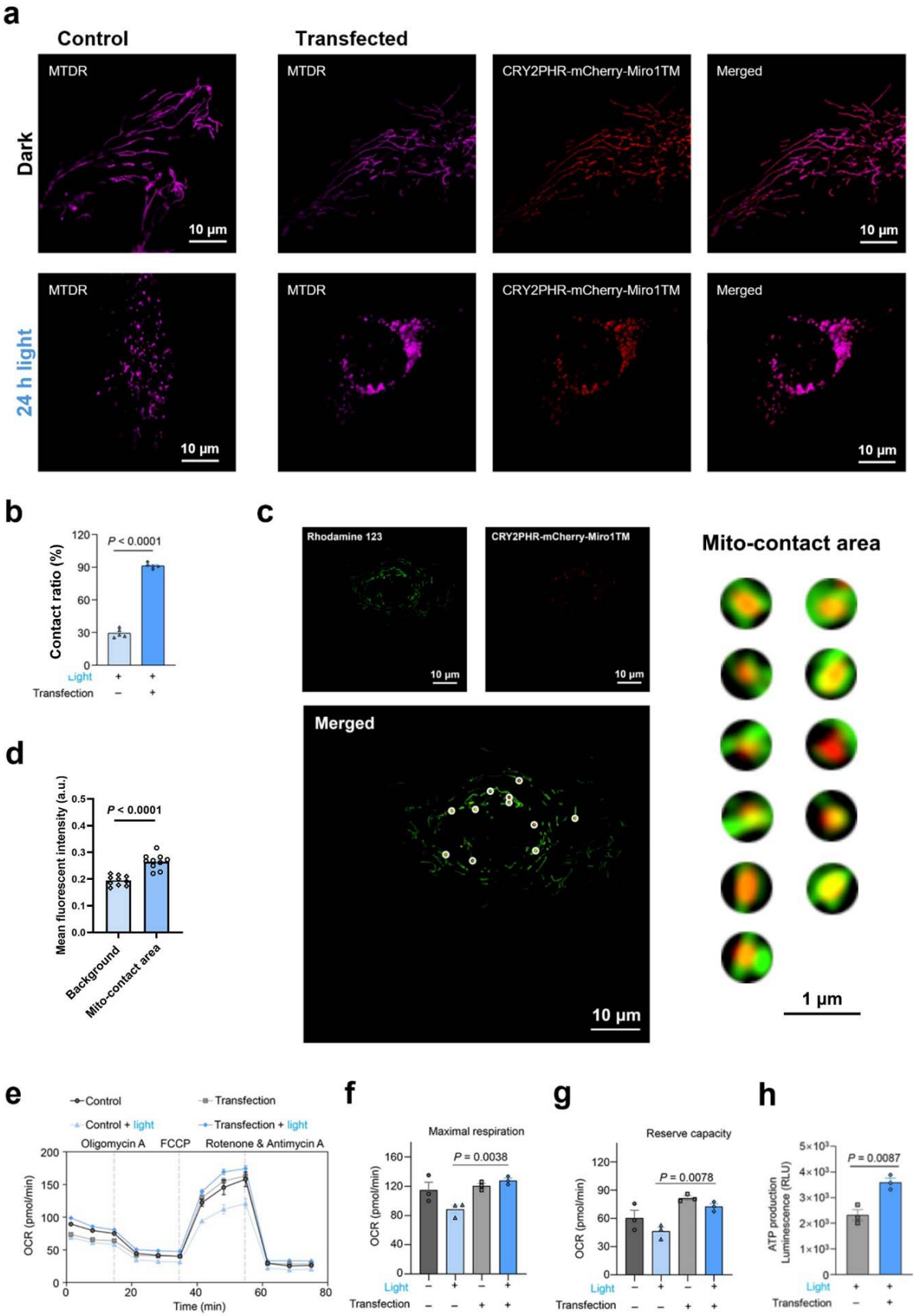
a
Control
Transfected
Dark
24 h light
MTDR
CRY2PHR-mCherry-Miro1TM
Merged
10 μm
b
Contact ratio (%)
P < 0.0001
Light
Transfection
c
Rhodamine 123
CRY2PHR-mCherry-Miro1TM
Merged
Mito-contact area
1 μm
d
Mean fluorescent intensity (a.u.)
P < 0.0001
Background
Mito-contact area
e
Control
Transfection
Control + light
Transfection + light
Oligomycin A
FCCP
Rotenone & Antimycin A
OCR (pmol/min)
Time (min)
f
Maximal respiration
P = 0.0038
g
Reserve capacity
P = 0.0078
h
ATP production Luminescence (RLU)
P = 0.0087

Figure 3. Mito-contacts preserve MMP for mitochondrial functions upon long-time blue-light eye damage

(a) Representative SIM images of living human retinal cells (ARPE-19) before and after exposed to blue light of 300 μW/cm^2 for 24 h with or within the transfection of CRY2PHR-mCherry-Miro1TM. Mitochondria stained with MTDR.

(b) The percentage of mitochondria contact ratio corresponding to (a). Data are given as *M* ± *SEM* (*n* = 5).

(c) Representative SIM images of transfected + 24 h light exposed ARPE-19 cells staining with Rhodamine 123 to reveal real-time MMP in a live cell and the zoom in images are mito-contact area.

(d) Relative MMP between whole cells and mito-contact area (CRY2PHR aggerate dots enriched area) corresponding to (c). Data are given as *M* ± *SEM* (n = 10).

(e) The real time OCR curves of ARPE-19 cells expressing CRY2PHR-mCherry-Miro1TM in mitochondria stress test. The OCR measured before the addition of oligomycin A represents the basal respiration of the cells; the OCR measured after the injection of FCCP reflects the maximal mitochondrial respiration capacity; and the OCR measured after the injection of rotenone and antimycin A represents non-mitochondrial respiration. Data are given as *M* ± *SEM* (*n* = 3).

(f) The OCR of maximum respiration (i.e., cells' maximum achievable respiration rate) of ARPE-19 cells after different treatments.

(g) The OCR of the reserve capacity (i.e., the capability of the cell to respond to an energetic demand) of ARPE-19 cells after different treatments.

(h) The ATP production of ARPE-19 cells after 24 h light exposure. Data are given as *M* ± *SEM* (*n* = 3). Statistical differences between the experimental groups were analyzed using a double-tailed Student's t test. All P values less than 0.05 were considered to indicate statistical significance.

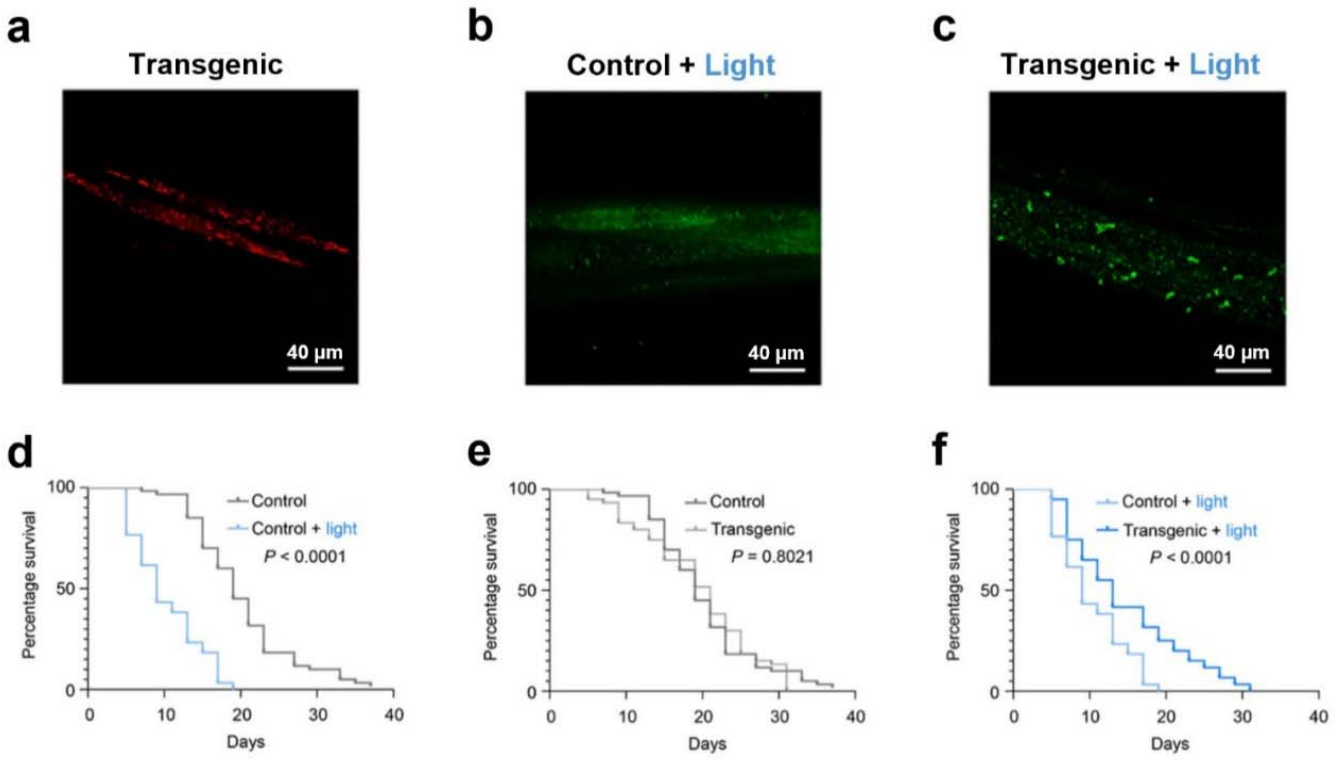

Figure 4. Mito-contact system extends lifespan of *C. elegans* under constant blue-light exposure

(a) The fluorescent image of *C. elegans* with the transgenic array containing CRY2PHR-mCherry-Miro1TM.

(b) The fluorescent image of *C. elegans* stained with MTG and exposed to blue light.

(c) The fluorescent images of *C. elegans* with the transgenic array containing CRY2PHR-mCherry-Miro1TM, stained MTG and exposed to blue light.

(d) Survival curves of control animals (n = 60) with or without exposure to blue light.

(e) Survival curves of animals (n = 60) with or without the CRY2PHR-mCherry-Miro1TM transgenic array.

(f) Survival curves of animals (n = 60) exposed to blue light with or without the CRY2PHR-mCherry-Miro1TM transgenic array.

Methods

Materials

MitoTracker™ Green FM (MTG, #M7514) and MitoTracker™ Deep Red FM (MTDR, #M22426) were obtained from Invitrogen (Thermo Fisher Scientific, USA). Penicillin–streptomycin (#15140163, 10,000 units/mL), fetal bovine serum (FBS, #26140079), DMEM (#11965092), DMEM/F-12 (#11320082) and geneticinTM selective antibiotic (#10131035) were all obtained from Gibco (Thermo Fisher Scientific, USA). Phosphate-buffered saline (PBS, #SH30256.01) was sourced from Hyclone (GE Healthcare Life Sciences, USA). CRY2PHR-mCherry-Miro1TM (Addgene plasmid, #102247) was a gift from Bianxiao Cui. TurboFect™ Transfection Reagent (#R0532), Invitrogen™ ATP Determination Kit (#A22066) and Rhodamine 123 (#R302) were purchased from Thermo Scientific (Thermo Fisher Scientific, USA). Cell Counting Kit-8 (CCK-8) was purchased from Dojindo (Dojindo Molecular Technologies, Inc., Japan).

Cell Culture and Transfection

The HeLa cell line, MCF-7 cell line, and HDFn cell line were cultured in DMEM supplemented with 10% FBS and 100 units/mL of penicillin-streptomycin. ARPE-19 cell line (arising retinal pigment epithelia, #CRL-2302, ATCC), were cultured in DMEM/F-12 supplemented with 10% FBS and 100 units/mL of penicillin-streptomycin. The cell cultures were maintained at 37 °C in a 5% CO2 cell incubator (Thermo Fisher Scientific, USA) with 100% humidity. Transfection was carried out utilizing TurboFectTM Transfection Reagent following the instructions provided by the manufacturer. We suggest using 2 μg CRY2PHR-mCherry-Miro1TM with 6 μL of TurboFect for 35 mm dish. The mixtures of DNA and transfection reagent were added dropwise to the cell cultures and incubated for 6 hours. After the incubation period, cell cultures were replenished with complete culture medium. To select the expressed cells, geneticin™ selective antibiotic at 500 ng/mL was treated with transfected cells.

Cell Imaging

Nikon Structured Illumination Microscopy (N-SIM, Nikon Corporation, Japan), a super-resolution microscope system was applied for live cell imaging in this study. The microscope was equipped with an Apochromat 100×/1.49 numerical aperture oil-immersion objective lens and solid-state lasers with wavelengths of 488 nm, 561 nm, and 640 nm. The output powers at the fiber end were set to 15 mW for each laser. The images were captured using Nikon NIS-Elements software, specifically the 512 × 512 resolution setting. Z-stacks were acquired with a step size of 0.2 μm. The raw images were then reconstructed and processed using NIS-Elements AR Analysis software (version AR5.11.00 64bit). The green channel images, which correspond to the emission bandwidth of 500-550 nm, were obtained by exciting the samples with a 488 nm laser specifically for MTG. The red channel images, which encompassed the emission bandwidth of 570-640 nm, were obtained by exciting samples with a 561 nm laser for mCherry. Additionally, the deep red channel images, covering the emission bandwidth of 660-735 nm, were captured by exciting samples with a 640 nm laser specifically for MTDR. Cells were seeded onto glass-bottomed culture dishes (MatTek; P35G-1.5-14-C) and allowed to adhere for 24 hours. Subsequently, staining with commercial dyes was conducted for a duration of 30 min. Both MTG and MTDR were prepared as 1 mM stock solutions in DMSO and diluted in complete culture medium to a final concentration of 50 nM for live-cell staining. Before imaging, the cells were washed three times with PBS. During illumination, a self-made blue light LED array with an intensity of 300 $\mu W/cm^2$ was employed. The subsequent analysis of the imaging data was carried out using ImageJ software.

The TEM images of cell slices were collected using a transmission electron microscopy (Hitachi HT-7800) with 80 kV.

Mitochondria Contact Ratio Quantification

Taking images of MTG or MTDR labeled mitochondria with SIM, ImageJ was then used to calculate the contacted area of CRY2PHR puncta or the distance between mitochondria. Based on the area or distance, the mitochondria were classified as either non-contact or contact. Contact ratio refers to the number of contact mitochondria by the total number of mitochondria.

Toxicity Test

The CCK-8 assay was used to assess cell viability following blue light exposure. A cell suspension (100 μL, containing 1,000 cells/well) was dispensed into a 96-well plate. After a 24-hour pre-incubation, the entire plate was irradiated with blue light for a specified duration, with the control group covered with aluminum foil. Subsequently, 10 μL of CCK-8 solution was added to each well, and the plate was incubated for an additional 1 hour. Absorbance at 450 nm was measured to determine cell viability.

Mitochondrial Morphology Quantification

Mitochondria were labeled with MTG or MTDR. After acquiring images using SIM, fluorescent images were imported into ImageJ. The image type was converted to 8-bit, and the threshold was auto adjusted. The area, shape descriptors, and threshold settings were refined using the “Set Measurements” function. Quantitative results were obtained through the “Analyze Particles” function. The “Aspect Ratio (AR)” value, calculated as the ratio of length to width (L/W), was recorded. Mitochondrial morphology was categorized into four groups based on AR values: Hyperfused ($AR \geq 5.0$), Tubular ($2.0 \leq AR < 5.0$), Intermediate ($1.5 \leq AR < 2.0$), and Round ($1.0 \leq AR < 1.5$).

Oxygen Consumption (OCR) Rate Assay

To assess the mitochondrial OXPHOS function in the presence of blue light exposure, the OCR of cells expressing CRY2PHR-mCherry-Miro1TM was measured using a Seahorse XFe-96 Analyzer (Agilent Technologies, USA). The OCR measurements were conducted in real time. Cells were divided into two groups: one group for blue light illumination and another group kept in the dark. Additionally, cells expressing CRY2PHR-mCherry-Miro1TM were also divided into two groups: one group for blue light illumination and another group kept in the dark. These cells were seeded into XFe-96 cell culture plates (Agilent Technologies, USA) at a density of 0.8 × 104 cells per well, using DMEM supplemented with 10% FBS. After a 48-hour incubation period, the culture medium was aspirated and replaced with pre-warmed unbuffered "Seahorse medium" (XF DMEM) at a pH of 7.4. The Seahorse medium was supplemented with 1 mM sodium pyruvate, 10 mM glucose, and 2 mM L-glutamine. Prior to the measurement, one group of cells and one group of cells expressing the plasmid were subjected to blue light exposure at an intensity of 300 $\mu W/cm^2$. Subsequently, the OCRs of the cells were evaluated using the XF Cell Mito Stress Test Kit (Agilent Technologies, USA), following the instructions provided by the manufacturer. In certain cases, the cells were subjected to treatment with specific compounds from Agilent Technologies, including 1 μM oligomycin A (an electron transport inhibitor), 2 μM FCCP (an electron chain transport accelerator), and 500 nM rotenone (a complex I inhibitor) with 1 μM antimycin A (a complex III inhibitor).

ATP Quantification Assay

ATP quantification was performed using the Invitrogen™ ATP Determination Kit. Two experimental groups, each consisting of three independent samples, were prepared: control (not transfected) group and transfected (CRY2PHR-mCherry-Miro1TM) group. Cells were seeded overnight into Costar 96-well

plates (Corning, USA) for adherence. Transfection was then performed for transfected group, followed by a 24-hour incubation for plasmid expression. After a certain time of blue light exposure, the samples were harvested and processed according to the manufacturer's protocol of the ATP Determination Kit. Luminescence was measured using a microplate reader (BioTek Instruments, Inc., USA).

Mitochondria Membrane Potential

Rhodamine 123, a cell-permeant, cationic, green-fluorescent dye, was used to stain mitochondria in living cells, with fluorescence changes dependent on the membrane potential. Rhodamine 123 was added to the cell samples to achieve a final concentration of 1 μM, and staining was carried out for 30 minutes. The cells were then washed three times with PBS. Images were captured using SIM.

Mito-contact Sites Identification and MMP Calculation

A custom image analysis algorithm was developed for study light induced mito-contact sites. The process begins by automatically detecting protein aggregates as distinct red puncta in the red fluorescence channel, accomplished by applying a high-percentile intensity threshold to identify the brightest local maxima. Following detection, a circular region of interest with a 10-pixel radius is defined around the center of each punctum, designated as the "mito-contact site." To ensure the analysis is restricted to mitochondria, a binary mask is generated from the corresponding green fluorescence channel. The algorithm then calculates the mean green fluorescence intensity (representing MMP) within the mitochondrial pixels of each mito-contact site and compares this value to the average intensity of the background, which is defined as all mitochondrial areas located outside of these specific sites. The code could be found in https://github.com/eugenelet/Modulating-inter-mitochondrial-contacts-to-increase-membrane-potential.

RNA-Sequencing and Data Analysis

Two groups (control and transfected), with each of six dishes, were prepared. Three for dark and three for blue light treatment ensured three independent repeats for each condition. HeLa cells were seeded to 60 mm dish and incubated for 24 h for adhering. Did transfection process for transfected group samples and waiting for 24 h for good expression. The blue light treatment group were exposure under blue light for a certain time before it was fixed. Then, all dishes were washed with cold PBS three times and fixed with lysis buffer for RNA extraction. Total RNA extraction and directional polyA RNA-seq were performed by the Genomics, Epigenomics and Sequencing Core at the University of Cincinnati [80].

The RNA quality was assessed using a Bioanalyzer (Agilent, USA), confirming high RNA quality. PolyA RNA was enriched using the NEBNext Poly(A) mRNA Magnetic Isolation Module (New England BioLabs, USA) combined with the SMARTer Apollo automated NGS library prep system (Takara Bio USA, USA) using 1 μg of total RNA as input. Library preparation was carried out using the NEBNext Ultra II Directional RNA Library Prep Kit (New England BioLabs, USA) with 8 PCR cycles. Following library quality control via Bioanalyzer and quantification using real-time qPCR (NEBNext Library Quant Kit, New England BioLabs, USA), individually indexed libraries were pooled proportionally and sequenced using the NextSeq 550 sequencer (Illumina, USA). Approximately 25 million reads per sample were generated. Fastq files for downstream data analysis were automatically generated via the Illumina BaseSpace Sequence Hub following sequencing. Differential expression analysis was conducted using the DESeq2 R package. Genes were considered significantly differentially expressed if the adjusted p-values (q-values) were less than 0.05. Mitochondrial genes were screened out by using Human MitoCarta3.0: 1136 mitochondrial genes. Gene set enrichment analysis (GSEA)

was performed using the GSEApy Python package. We used pre-ranked gene expression data to assess overrepresented Gene Ontology (GO) categories and Kyoto Encyclopedia of Genes and Genomes (KEGG) categories. Specially, we analyzed three GO categories – Biological Process, Molecular Function, and Cellular Component – from GO gene subsets respectively; and also analyzed KEGG pathway for the wider range of biochemical processes.

C. elegans Experiments

Strains and Maintenance: The animal experiments were approved by the Cincinnati Children's Hospital Medical Center Institutional Biosafety Committee. Nematode growth medium (NGM) was used for *C. elegans* culture and all maintenance and experiments were carried out at 20 °C. OP50 Escherichia coli was used as a food source for all experiments. Egg-lay-synchronized hermaphrodite animals were used for all experiments at the stage noted. Strain ZAC307 cchEx307[pTG028_eft-3p::CRY2::-mCherry-Miro1TM + myo-2p::RFP] expresses CRY2-mCherry-Miro1TM in all cells. ZAC307 was created by injecting N2 Young adult worms with a mix containing 0.25 mM EDTA, 2.5 mM Tris-Cl, 10 ng µl−1 pTG028[eft-3p::CRY2::-mCherry-Miro1TM] plasmid, 2.5 ng µl−1 myo-2p::RFP plasmid, 90 ng µl−1 NEB 1kB ladder. Offspring were selected for the presence of the transgenic array based the red pharyngeal myo-2p::RFP marker. The expression of CRY2::-mCherry-Miro1TM was verified in L4 worms with a Nikon A1R Confocal at 60× using the 60× Apo λ S Oil Immersion Objective.

Lifespan Analysis: For the lifespan study, four groups of *C. elegans* were used. On day 0, L4 animals were transferred to 3 × 60 mm NGM plates, 20 animals per plate (n = 60). For the Control group, N2 (wild-type) animals were kept in a box, in darkness at 20 °C. For the Control + light group, N2 (wild-type) animals were kept in a blue light box (300 µW/cm^2) at 20 °C. For the Transgenic group, array

positive ZAC307 animals were kept in a box, in darkness at 20 °C. For the Transgenic + light group (optogenetic treatment), array positive ZAC307 animals were kept in the blue light box (300 μW/cm^2) at 20 °C. Every two days, each set of 20 adult animals was moved to a new 60-mm NGM plate to leave any progeny behind, and the number of living animals was assessed. Animals were counted as living if they moved or responded to stimuli when they were picked or tapped.

Data Analysis

Statistical analysis was conducted using either Student's t-test or Log-rank (Mantel-Cox) test only for the survival analysis of the worm. The data were presented as mean ± standard error of the mean (SEM). Statistical analysis and graphing were performed using Prism 8 software (GraphPad) or Excel (Microsoft). Image analysis was carried out using ImageJ-win64 software (NIH Image). The final assembly of images was done using PowerPoint (Microsoft).

Statistics and Reproducibility

Statistics were performed in Prism 8 (GraphPad). No data was excluded from the analysis. No statistical method was used to pre-determine sample size. Within experimental groups, samples were randomized for each experimental replicate. The investigators were not blinded to allocation during experiments and outcome assessment. Data distribution was assumed to be normal, but this was not formally tested, therefore data distributions are visualized in each figure.

Data Availability

All data supporting the findings of this study are available either in the article and/or its Supplementary Information files. Source data are provided with this paper.